Journal of Magnetic Resonance 214 (2012) 346–351

Contents lists available at SciVerse ScienceDirect

Journal of Magnetic Resonance

journal homepage: www.elsevier.com/locate/jmr

Communication

Coherent NMR Stark spectroscopy

Matthew R. Tarasek, David J. Goldfarb, James G. Kempf *

Department of Chemistry & Chemical Biology and Center for Biotechnology and Interdisciplinary Studies, Rensselaer Polytechnic Institute, Troy, NY 12180, United States

ARTICLE INFO

Article history:
Received 23 September 2011
Revised 26 November 2011
Available online 7 December 2011

Keywords:
Stark effect
Quadrupole interaction
Coherent averaging
Gallium arsenide (GaAs)

ABSTRACT

We demonstrate phase-coherent Stark effects from a radiofrequency E field at twice the NMR frequency ($2\omega_0$) of ^{69}Ga in GaAs. The $2\omega_0$ phase (ϕ_E) selects component responses from the nuclear quadrupole Hamiltonian ($\mathcal{H}_Q$). This is possible by synchronizing few-μs $2\omega_0$ pulses with an NMR line-narrowing sequence, which averages the Stark interaction to dominate spectra on a background with $10^3\times$ enhanced resolution. Spectra vs ϕ_E reveal relative sizes of tensorial factors in $\mathcal{H}_Q$. Comparative modeling and numerical simulations evaluate spectral features unexplained by average Hamiltonian theory, and suggest improvements for quantitative calibration of individual response components. Application of this approach to bulk samples is of value to define Stark responses that may later be used to interrogate the internal electrostatics of structured samples.

1. Introduction

Coherent manipulation of spins is the signature feature of nuclear magnetic resonance (NMR). Such control takes NMR beyond usual spectroscopic identification of energy spacings and into a world of complex multidimensional spectra with dramatically enhanced information content. Coherent methods allow transfer of spin order between vicinal nuclei for multidimensional correlation spectra, as well as the tailoring of effective Hamiltonians ($\mathcal{H}_{\text{eff}}$) for exclusive focus on target spin interactions. With these, NMR provides atomic detail on structure, chemical environment and dynamics within a wide variety of material and molecular systems.

Tools for coherent NMR are dominated by radiofrequency (rf) magnetic pulses. Yet *electrical* interactions determine much of the spectral variety that makes NMR so broadly informative. Intra-sample electric (E) fields establish spin-by-spin variations in the NMR Hamiltonian, most notably, for chemical-shift and quadrupole interactions. However, E-field-induced changes in NMR spectra (Stark effects) have rarely been observed in a direct, controlled manner [1–5], while coherent response (e.g., accounting for both amplitude and *phase* of an oscillating E field) has never been demonstrated. Thus, lacking calibrated effects, much less their coherent modulation, electrostatics characterization remains elusive to NMR.

Here, we develop a promising new approach using phase-coherent quadrupolar Stark effects (QSEs) from an rf E field applied at twice the NMR frequency ($2\omega_0$) for ^{69}Ga in GaAs. We utilize the phase coherence to define directional components of the response without reorienting the sample. QSE-induced changes are observed at 10^3-fold enhancement over the natural linewidth using a POWER (Perturbations Observed With Enhanced Resolution) NMR format [6–8]. In general, POWER methods synchronize a pulsed sample perturbation (here, the $2\omega_0$ E field) with a sequence of $\pi/2$ pulses that provide the narrowing. The spectrum is then dominated by the selectively averaged perturbation Hamiltonian, presently the conversion of the $2\omega_0$ QSE to a secular form in which the phase selects the component of tensorial response to be measured.

Extensions of this approach will enable needed NMR elucidation of functional electrostatics. For example, the atomic-scale details of variable internal E fields can be used to guide development of material devices. However, very few NMR studies have been able to map local electrostatics, e.g., near point defects, interfaces or surfaces. In addition, experimental views of intramolecular electrostatics have been essentially the sole domain of vibrational spectroscopy [9], whereas site-specific chemical and structural information is far more prevalent from NMR. Finally, by defining the impacts of E fields on chemical shifts or quadrupole couplings, electrostatic observations may extend the empirical basis of NMR models that connect spectral appearance to molecular structure [10] or quadrupolar relaxation with dynamics.

Regardless of the specific target, the first step is calibration of responses from *bulk* samples. That enables subsequent definition of electrostatics within *structured* samples. This is well known in vibrational spectroscopy [9,11]. There, pre-calibration of Stark effects from E fields applied to molecular crystals has allowed electrostatic analysis of spectra from the molecule as a ligand. For example, differential free and bound spectra then report on the intramolecular E fields of the binding partner. In principle, NMR may also achieve this, and with a potentially wider array of

* Corresponding author. Address: RPI, Department of Chemistry, 110 8th Street, 209a Cogswell Lab, Troy, NY 12180, United States. Fax: +1 518 276 4887.
E-mail address: kempfj2@rpi.edu (J.G. Kempf).

1090-7807/$ - see front matter © 2011 Elsevier Inc. All rights reserved.
doi:10.1016/j.jmr.2011.11.018

non-perturbative, isotopically labeled probe moieties. Similarly, this general approach can be used to evaluate local, internal structures in material systems. For example, QSEs have been used in this manner to map E fields about point defects and interfaces in an AlGaAs/GaAs heterojunction [7], results enabled by prior knowledge of the bulk response from an applied E field. Possibilities for likewise measuring molecular QSEs have also been demonstrated [12,13]. However, even with modernization of NMR instruments and many related methods, any broader use of NMR Stark effects has been limited by challenges of resolution, as typical effects are orders of magnitude less than solid-state linewidths. Our application of resonant QSEs in general, and the POWER method in specific, aims to defeat that challenge.

The earliest of the rare observations of NMR Stark effects were anticipated by Bloembergen's consideration of quadrupole couplings [1]. Just prior to that, Stephen [14] and Buckingham [15] provided models for smaller, but still significant effects on chemical shift. Realization of QSEs from applied fields (**E**) soon followed [2,3], whereas chemical-shift response to an intramolecular **E** was attributed much later [16]. From the beginning, Bloembergen noted the possibility of QSEs from both *static* and *resonant rf E* fields. Either distorts the E-field-gradient tensor ($\nabla\mathbf{E}$) at noncentrosymmetric sites. The nuclear quadrupole Hamiltonian ($\mathcal{H}_Q$), whose terms are proportional to the five unique components of $\nabla\mathbf{E}$, then exhibits linear response vs $|\mathbf{E}|$. Because the radiofrequency is far below electronic Bohr frequencies, the magnitudes of rf and static QSEs are identical.

The resonant rf effects correspond to single or double-quantum transitions from oscillation of $\mathcal{H}_Q$ at ω_0 or $2\omega_0$. These are particularly valuable for defining tensorial response. Normally, that requires rotation to position a particular component of $\nabla\mathbf{E}$ with the lone secular (static) term in $\mathcal{H}_Q$. Meanwhile, the four other unique tensor components are paired with nonsecular terms at $\pm\omega_0$ or $\pm2\omega_0$. Of course, the latter relate to resonant QSEs. Thus, characterization at zero, ω_0 and $2\omega_0$ can obviate rotational studies. This frequency dependent approach was indirectly demonstrated by separate studies from Gill and Bloembergen (GB) [3], using static **E** to induce a linear spectral splitting, and from Brun et al [4,5] using a $2\omega_0$ field to induce a steady state population distribution that is saturated relative to thermal equilibrium, a nonlinear (Lorentzian) response vs $|\mathbf{E}|$. The two-frequency results from these groups were consistent with accepted theory for cubic GaAs, where the QSE follows geometric scaling of a single response parameter, C_{14} [2–6,17]. More recently [17,18], we used steady state $2\omega_0$ QSEs to quantify C_{14} and map tensorial response over 90° of rotation and 10-fold range of $|\mathbf{E}|$. This gave first detailed confirmation of theory, a firm milestone towards extended applications to lower-symmetry systems.

2. Theoretical basis

The rf phase (ϕ_E) had no role in original descriptions of resonant QSEs. That was appropriate for the magnitude response inherent to steady state excitation [4,5,17]. However, later analysis by Kempf and Weitekamp noted a definite part for ϕ_E using POWER NMR [6,8]. It sinusoidally varies the pairing of spin operators with components, V^{in}_{xy} and $\eta'^{in} = (V^{in}_{xx} - V^{in}_{yy})/2$, of the induced $\nabla\mathbf{E}$ in [6,8]

$$\widetilde{\mathcal{H}}'_{Q2} = \frac{\xi_Q}{2}\left[\cos\phi_E(\eta'^{in}I^2_{xy} + V^{in}_{xy}[I_x, I_y]_+) + \sin\phi_E(\eta'^{in}[I_x, I_y]_+ - V^{in}_{xy}I^2_{xy})\right], \tag{1}$$

the secular portion of the $2\omega_0$ QSE (in Hz), where $\xi_Q = eQ/(2I(2I-1)h)$, I and Q are the nuclear spin and quadrupole moment, e and h have standard meaning, $I^2_{xy} = (I^2_x - I^2_y)$ and $[I_x, I_y]_+$ is an anticommutator. The POWER sequence of Fig. 1a interleaves few-μs pulses of the $2\omega_0$ E field (i.e., evolution under $\widetilde{\mathcal{H}}'_{Q2}$) within

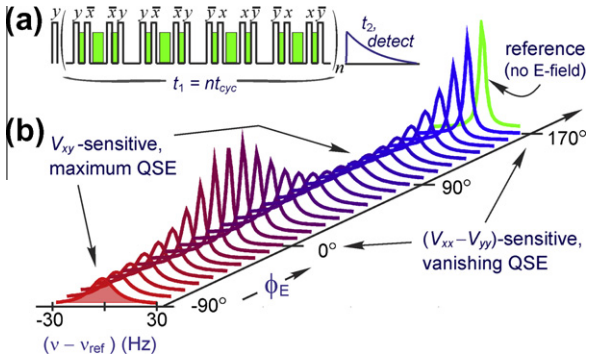

Fig. 1. Coherent Stark effects from $2\omega_0$ POWER NMR. (a) Sequence of $\pi/2$'s with triplet pulses of $2\omega_0$ E-field (shaded) at phase ϕ_E. (b) Stacked ^{69}Ga spectra from Fourier transformation of t_1 using (a) with $|\mathbf{E}| \sim 100$ V/cm. Each spectrum had distinct ϕ_E: at −90° (shaded at front), the QSE reports on V^{in}_{xy}. Proceeding to $\phi_E = 0°$ selects instead for $(\eta)^{in}$, which vanishes for a lineshape matching the reference at back.

a few-100-μs sequence of $\pi/2$ pulses. The pattern of phases for *both* pulse types averages $[I_x, I_y]_+$ to zero, and I^2_{xy} to a new form, $\frac{\tau'}{\tau}I^2_z$ [8], where $\frac{2\tau'}{3\tau}$ is the $2\omega_0$ duty factor over the duration ($t_{cyc} = 24\tau$) of the full sequence.

This 'extraction' focuses the selectivity of ϕ_E in

$$\overline{\mathcal{H}}^{(0)}_{Q2} = \frac{\tau'}{2\tau}\xi_Q(\eta'^{in}\cos\phi_E - V^{in}_{xy}\sin\phi_E)I^2_z, \tag{2}$$

the zeroth-order result from application of average Hamiltonian theory (AHT) to the full POWER sequence. Net evolution under $\overline{\mathcal{H}}^{(0)}_{Q2}$ predicts a quadrupole splitting, with adjacent peaks separated by ν_{Q2}, which is twice the coefficient of I^2_z in Eq. (2). AHT further predicts that $\overline{\mathcal{H}}^{(0)} = \overline{\mathcal{H}}^{(0)}_{Q2}$, i.e., the overall average Hamiltonian is free of contributions from 'background' dipole–dipole, chemical-shift and $\mathcal{H}_Q$ interactions. Thus, the resolution limit of QSE-induced features is set, in principle, by the width of a reference spectrum obtained without $2\omega_0$ pulses.

3. Materials and methods

3.1. Sample and $2\omega_0$ POWER experiments

Details of apparatus and sample are as recently presented [8,17,18]. Briefly, we used a single-crystal, high-resistivity, undoped GaAs sample of 380 ± 25 μm thickness along the [001] growth axis. This axis was aligned with a static magnetic field of $|\mathbf{B}_0| = 14.1$ T, for ω_0 (^{69}Ga) $\sim (2\pi) \times 144.12$ MHz. The sample was maintained at room temperature. Assessment of the E-field amplitude was as described [17] with recent improvements [18]. POWER NMR of the $2\omega_0$ QSE was according to earlier design, including protocol to establish two-channel phase coherence between ω_0 B_1 and $2\omega_0$ E fields [8]. Here, we used $t_{90} = 4.0$-4.6 μs and cycle time $t_{cyc} = 408$ μs for the CLSW-16 [19] multiple-pulse line-narrowing sequence. Similar results were obtained with $t_{cyc} = 200$ μs.

Time-domain spectra in $t_1 = n \times (n_{incr}\, t_{cyc})$ were formed by integration of real-time signal transients in t_2. A typical spectrum (i.e., from the series in Fig. 1b) consisted of 150 complex points in t_1 at intervals of $n_{incr}\, t_{cyc}$. For $n_{incr} = 3$ and t_{cyc} 408 μs, spectral width was $sw_1 = 817$ Hz and $t_{1,max} = 184$ ms. Time-proportional phase incrementation (TPPI, [20]) was applied to the $\pi/2$ preparation pulse to provide apparent shift to $sw_1/4$, avoiding any need to distinguish dc artifacts from the otherwise zero frequency signal. Fourier transformation in t_1 yielded a Lorentzian lineshape,

$$L(\nu) = \frac{a_0\Delta\nu^2}{\Delta\nu^2 + 4(\nu - \nu_0)^2} \tag{3}$$

of amplitude a_0, position ν_0 and FWHM $\Delta\nu$. Reference spectra obtained without synchronized $2\omega_0$ *E*-field pulses typically had $\Delta\nu = (\Delta\nu_{ref} = 3–5$ Hz). For 'Stark-active' experiments, $2\omega_0$ pulses (synchronized as in Fig. 1a) had durations $0.8\,(t_{cyc}/24 - t_{90})$, i.e., 80% of the maximum possible without overlapping the $\pi/2$ pulses. The corresponding $2\omega_0$ duty factor was ~0.4 for the full sequence (Fig. 1a). To avoid arcing to the NMR coil, we limited tests to fields $\leqslant$1 kV/cm. Constant-power format [21] was used for both $\pi/2$ and $2\omega_0$ pulses, entailing repetition of the POWER sequence $(t_{1,max} - t_1)/t_{cyc}$ times at the start of the 1.5 s recycle delay. For spectra of Fig. 4(b), fixed rf magnetic pulse durations were used and powers were adjusted to vary the pulse angle. Home-written *Mathematica* code was used to process and analyze all experimental data, as described earlier [8,17].

As briefly discussed ahead, benefits of 2nd-averaging from select pulse-timing offsets (Refs. [8,21]) were explored to $t_{off} = 60$ ns (yielding 185 Hz frequency offset), but yielded no noticeable differences vs spectra presented here, all obtained with $t_{off} = 0$. Spectra from phase-stepped [21] versions of the $2\omega_0$ POWER experiment were likewise indistinguishable. Shaped $2\omega_0$ pulses were also tested as a means to mitigate any effect of phase and amplitude transients, but showed only the expected reduction in QSE response due to altered integrated pulse areas. These results will be detailed elsewhere.

4. Numerical simulations

All simulations were run using gamma [22] version 4.1.2, which updates obsolete c++ syntax relative to v4.1.1. Source code was provided by Prof. Matthias Ernst of the ETH (Zurich), and is also now available as gamma 4.3 (with significant speed enhancements) as part of the modernization of the GAVA [23] application into the VESPA package (http://scion.duhs.duke.edu/vespa/). The spin system is similar to that described earlier for ^{69}GaAs [21], excepting that we used 5 spins (rather than 6) to avoid a memory overrun on our 8 GB-RAM system. The omitted atom is the 'below-plane' site from the earlier set. To compensate the corresponding loss of dipole–dipole interactions, we decreased the lattice spacing to a smaller fraction of the natural value ($a^* = 0.63a$ vs $0.73a$ earlier). The reduced symmetry of the set and larger pairwise couplings explain the non-Gaussian starting lineshape (left inset of Fig. 3). Other 5-spin models (e.g., including ^{71}Ga) did not improve upon the spectral appearance. The density matrix for the initial condition was $\sum_i \gamma_i I_{z,i}$, with i encompassing both nuclear species, and the detection operator was $\sum_j I_{+,j}$ with j covering ^{69}Ga only. Relaxation was not included.

Pulse sequences and sum-over-spins Hamiltonians were coded in house, including all hetero- and homonuclear dipolar interactions ($\mathcal{H}_D$), as well as the $2\omega_0$ QSE [$\widetilde{\mathcal{H}}'_{Q2}$ of Eq. (1)]. Evolution was from the summed $\mathcal{H}_D$, its simultaneous influence during finite-width $\pi/2$ pulses, and, for POWER simulations, $\widetilde{\mathcal{H}}'_{Q2}$, which, due to its resonant nature, was summed over ^{69}Ga sites only. Eq. (1) for $\widetilde{\mathcal{H}}'_{Q2}$ is a rotating-wave approximation that omits terms oscillating at $\pm 4\omega_0$. No other approximations were applied, e.g., $[I_x, I_y]_\dagger$ terms were included even though they do not contribute to $\overline{\mathcal{H}}^{(0)}_{Q2}$. We do note that, in the assumed sample geometry $\eta^{in} = 0$. Thus, for simulations at $\phi_E = 90°$, the $[I_x, I_y]_\dagger$ terms of $\widetilde{\mathcal{H}}'_{Q2}$ are multiplied by zero (Eq. (1)). However, at $\phi_E = 45°$ their contribution is finite. Yet simulations there were identical to those at $\phi_E = 90°$, provided that we scaled $|\mathbf{E}|$ by $(\sin 45°)^{-1}$ to maintain the amplitude of the I^2_{xy} contribution. Thus, the $[I_x, I_y]_\dagger$ term appears to be ineffectual, even outside of AHT. Finally, sequence details for line-narrowing and POWER simulations followed experiments, including TPPI implementation. Processing and analysis with *Mathematica* was essentially identical to that applied with experimental data.

5. Results and discussion

The elevated role of ϕ_E in $2\omega_0$ POWER NMR is detailed by Eq. (2) and discussion in Theoretical Basis. We demonstrate the results in Fig. 1b, a series of ^{69}Ga spectra collected as a function of the $2\omega_0$ phase. QSE-dependent redistribution of intensity from the peak center is consistent with introduction of quadrupole satellites. For $\phi_E = \pm 90°$, where $\overline{\mathcal{H}}^{(0)}_{Q2}$ is sensitive only to V^{in}_{xy}, maximal distinction from the reference occurs. In contrast, Eq. (2) shows that $\phi_E = 0$ or 180° instead selects η'^{in}, and corresponding spectra from Fig. 1b appear as if no *E* field had been applied. These results are explained by the chosen GaAs geometry (crystalline [0 0 1] coparallel with $\mathbf{B}_0$ and $\mathbf{E}$), for which one expects $V^{in}_{xy} = C_{14}|\mathbf{E}|$ and vanishing η'^{in}. Intermediate ϕ_E values yield QSEs according to sinusoidal combination of V^{in}_{xy} and η'^{in}. This quickly obtained series vs ϕ_E (requiring ~1 h) provided what would otherwise require a rotation study of (generously) ~10 h. Further, ϕ_E is trivially set [8], in contrast to rotation, which disturbs both sample and the tuned/matched $2\omega_0$ circuit, while requiring added goniometric hardware, which is both an inconvenience and a complication for evaluation of $|\mathbf{E}|$ [17]. The phase-coherent approach is also far more efficient than frequency dependent assessment of tensorial response, which would necessitate a variety of apparatus, experiment types and formats for data analysis.

We evaluated the phase-coherent response from Fig. 1b via plots of corresponding fit parameters in Fig. 2. The QSE may be interpreted as spectral broadening, $\Delta\nu_{Q2} = (\Delta\nu - \Delta\nu_{ref})$, in a single Lorentzian (SL) model [Eq. (3)]. Fig. 2a–c plots ϕ_E variations of co-fitted $\Delta\nu$, a_0 and ν_0, the SL width, amplitude and position of individual spectra, while (d) provides corresponding χ^2 values. The sinusoidal pattern of $\Delta\nu_{Q2}$ follows $|\overline{\mathcal{H}}^{(0)}_{Q2}|^2$, and is well fit by $(13.1 \pm 0.1$ Hz$)\sin^2\phi_E$. Spectral area is constant, thus a_0 falls as $\Delta\nu_{Q2}$ rises (Fig. 2b). Finally, variation of ν_0 with ϕ_E (Fig. 2c) is unexplained, but occurred independent of the order of spectral acquisition, and tracks as the square of the $2\omega_0$ Hamiltonian, similar to Bloch–Siegert shifts from magnetic excitation.

A modified-AHT model reproduces spectral behavior at similar quality to the noted SL fits. For spin-3/2 ^{69}Ga, zeroth-order AHT ($\overline{\mathcal{H}}^{(0)}_{Q2} \propto I^2_z$) predicts a 3:4:3 triplet of central and satellite transitions. Broadening such triplets as $|\overline{\mathcal{H}}^{(0)}_{Q2}|^2$ yields a model nearly identical to the fitted SLs, as shown in Fig. 2e and f for spectra at $\phi_E = -92$ and 28°. These are consistent with triplet splitting linear in $\overline{\mathcal{H}}^{(0)}_{Q2}$ [$\nu_{Q2} = (4.7 \pm 0.3$ Hz$)\sin\phi_E$], and broadening as $\Delta\nu'_{Q2} = (8.5 \pm 1$ Hz$)\sin^2\phi_E$. The overall consistency with experiments vs ϕ_E is shown in Fig. 2(a-d). There, along with earlier treatment of data, we plot parameters of SL fits *to simulated triplets*, which were formed using noted ν_{Q2} and $\Delta\nu'_{Q2}$ dependencies in

$$F(\nu) = 3L'(\nu - \nu_{Q2}(\phi_E)) + 4L'(\nu) + 3L'(\nu + \nu_{Q2}(\phi_E)) \tag{4}$$

where L' has the form of Eq. (3) but replacing $\Delta\nu$ with $(\Delta\nu'_{Q2}(\phi_E) + \Delta\nu_{ref})$. Thus, while simulated spectra vs ϕ_E obviously are triplets, the high quality of SL fits to the series underscores the concealment of that nature by concurrent broadening. The progressions of SL parameters $\Delta\nu_{Q2}$ and a_0 from fits to these simulations follow those from SL fits to experimental data. Interestingly, so does χ^2. Thus, the modified-AHT model of Eq. (4) reproduces ϕ_E-dependent discrepancies with SL fits. The latter work best ($\chi^2 \sim 1$) when triplets coalesce to a single peak at the smallest QSEs ($\sin\phi_E \sim 0$), and again for the largest ($|\sin\phi_E| \sim 1$), where quadratic broadening overwhelms linear splitting.

Key support for this model comes from numerical simulations of density matrix evolution. Fig. 3 presents results using a 5-spin ($3 \times$ Ga, $2 \times$ As) accurate representation of ^{69}GaAs [21], with simulated evolution from constant dipole–dipole interactions, finite-width $\pi/2$ pulses, and, where $2\omega_0$ pulses appear, $\widetilde{\mathcal{H}}'_{Q2}$ of ^{69}Ga. Using sequence parameters as in experiments (Figs. 1 and 2), simulation

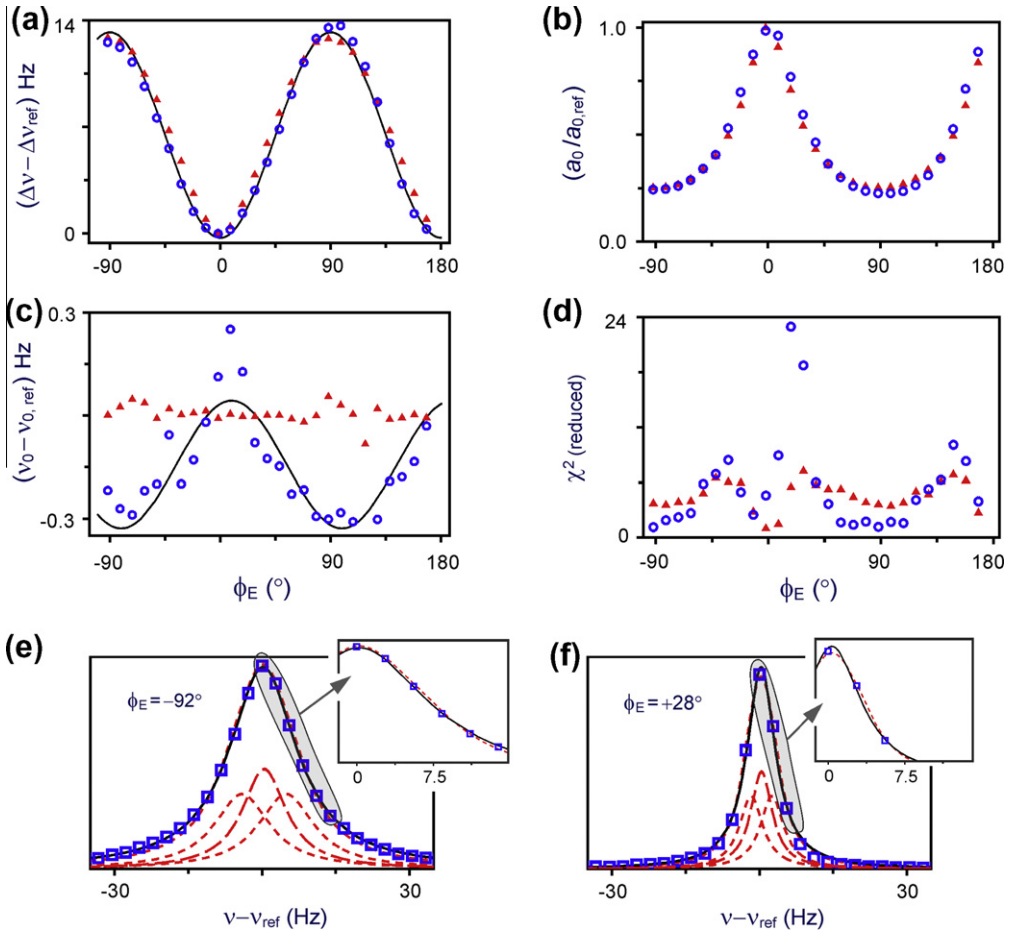

Fig. 2. Parameter variation vs ϕ_E. (a) QSE-induced broadening, $\Delta\nu_{Q2}$. Open circles (blue) are from fits of individual spectra in Fig. 1b to single Lorenztians (SLs). The solid curve is the fit of these values to $(\Delta\nu_{Q2,max} \times \sin^2\phi_E)$. Triangles (red) are from SL fits to simulated triplets with QSE-induced broadening. Overlapping patterns support the simulated model. (b–d) Similar plots of (b) amplitudes, a_0, (c) positions, ν_0, and (d) reduced χ^2 from the same SL fits. The curve in (c) is a sinusoidal fit. (e and f) Individual spectra at $\phi_E = -92°$ and 28°, each with both fit models [SL as solid curve, whereas the broadened triplet and its Lorentzian subcomponents are dashed (red)]. For (a–d), random noise was incorporated in simulated triplets on par with experiments, e.g., signal-to-noise ~300 at $\phi_E = 0°$. (For interpretation of the references to color in this figure legend, the reader is referred to the web version of this article.)

yielded a triplet with near-AHT splitting (4.3% low), plus 3.3 × non-AHT broadening of both central and satellite peaks relative to the simulated reference. The smaller splitting and increased widths mimic experimental observations, although with reduced severity.

Finally, the simulations also suggest that a return to AHT is possible. The upper right inset of Fig. 3 shows the result when using 2nd averaging, in particular, from a 150 Hz offset introduced via a previously described method [8]. Broadening relative to the reference simulation remained, but was reduced at central and satellite peaks by 1.2 and 1.7-fold compared to the non-2nd-averaged case. This provided fully resolved splitting now within <1% of AHT. This promises quantitative evaluation of $2\omega_0$ POWER spectra. However, the 2nd-averaging explored in experiments has not, thus far, returned AHT-like spectra. Offsets up to ~200 Hz yielded no change in lineshapes, nor did 'phase-stepped' 2nd averaging [21], even when combined with offsets. This may be due to numerical simulations capturing only a portion of the broadening, perhaps due to our necessarily simplified 5-spin representation of GaAs.

Nonetheless, QSE responses observed in experiments are robust to several factors. Foremost, Figs. 2 and 3 prove $\overline{\mathcal{H}}^{(0)}_{Q2}$ as a valid descriptor of *phase-coherent* response. Thus, by mere adjustment of ϕ_E, we succeeded in defining the relative QSEs in V^{in}_{xy} and η^{in}. Secondly, the potential to quantitate responses in individual tensor components is highlighted in Fig. 4a, which plots induced broadening as $\sqrt{\Delta\nu_{Q2}}$ vs $|\mathbf{E}|$. High-precision linear response ($R^2 = 0.9990$) was observed up to the maximum tested field (~1 kV/cm). Thus, a new, detailed model for the non-AHT broadening would enable calibration of individual components of the Stark response. Finally,

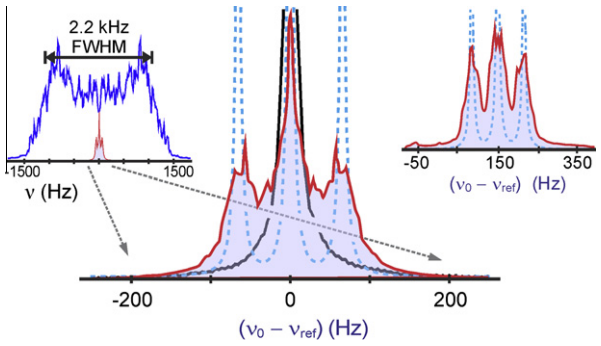

Fig. 3. Numerical simulations. Left inset: result from a (π/2-detect) sequence. The 2.2 kHz FWHM reproduces the dipolar width, and is thus an appropriate challenge for simulations of $2\omega_0$ POWER. There (shaded, expanded view at center), we used $V^{in}_{xy} = C_{14}|E|$, with $C_{14} = 2.6 \times 10^{12}$ m^{-1} [18], $|\mathbf{E}| = 600$ V/cm, and pulse sequence as in experiments. The result is a QSE-broadened triplet, shown with reference simulation [no $2\omega_0$ pulses (solid)] and AHT Q-split pattern (dashed). Right inset: improvement from concurrent 2nd-averaging shift of 150 Hz.

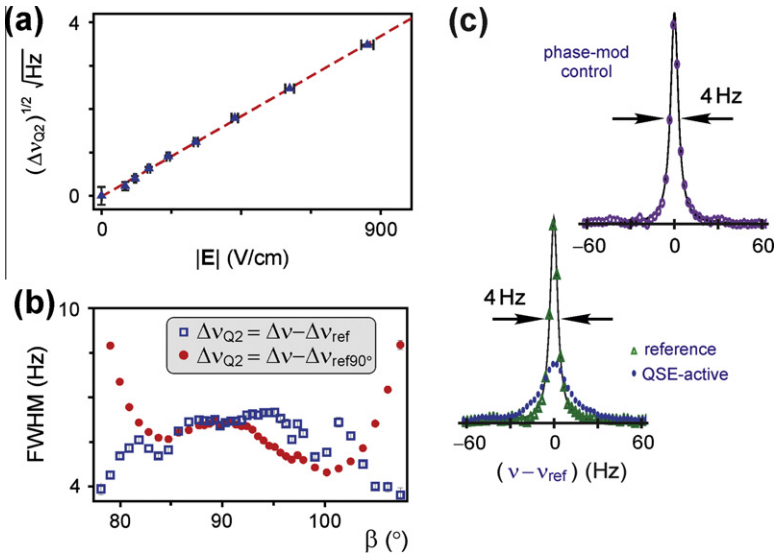

Fig. 4. Parameter variations and control at $\phi_E = 90°$. (a) Root added linewidth vs $|\mathbf{E}|$ from SL fits to ^{69}Ga spectra. The dashed line is a linear fit with $R^2 = 0.9990$. **(b)** Added width vs pulse angle β at fixed $|\mathbf{E}|$. When (naively) defining each $\Delta\nu_{Q2}(\beta)$ relative to the width ($\Delta\nu_{ref90°}$) of the reference spectrum at $\beta = 90°$ (closed circles), significant variations are apparent. However, these flatten (open squares) across $\beta \sim 85$–$95°$ when $\Delta\nu_{ref}(\beta)$ is properly determined with co-collected reference and Stark-active spectra at each β value. (c) Phase-modulated control, compared to reference and QSE-active spectra. The control used $\phi_E = -90°$ on alternate $2\omega_0$ pulse triplets, and matches the E-field-free reference lineshape. This cancelation of responses from adjacent triplets demonstrates the absence of Stark fluctuations faster than 1/4 of the full pulse sequence (~50 or 100 μs).

Fig. 4b shows results vs deviation of NMR pulse angles (β) from $\pi/2$. At constant pulse duration and fixed $|\mathbf{E}|$, the range $\beta \sim 85$–$95°$ yielded flat response (rmsd = 0.13 Hz, ~2% of $\Delta\nu_{Q2}$) relative to reference spectra with matching β. This avoids any misinterpretations that might occur with pulse-angle errors. It also explores QSE behavior across optima of the bare sequence: $\beta = 90°$ or 95° in the present implementation [21]. However, no β value changed the basic spectral shape from those appearing in Figs. 1 and 2.

We can discount several factors that might contribute to non-AHT spectral character. Phase transients in $2\omega_0$ pulses would spoil conversion of I_{xy}^2 to I_z^2. However, transients are not obviously apparent in our square pulse profiles. Further, to lessen any that might be present, we tested smoothly shaped (sine-lobe) $2\omega_0$ pulses, and found no change other than a reduced broadening exactly attributable to the smaller pulse areas. We also considered possible effects of $\mathbf{E}$ at ω_0, e.g., as must accompany rf magnetic pulses. However, the single-ω_0 QSE is 'doubly vanishing' in present experiments: first by geometry ($\mathbf{B}_0$//[001]) [6], and, even allowing misalignment, by its zero average Hamiltonian. Finally, even before invoking AHT, corrections to $\widetilde{\mathcal{H}}'_{Q2}$ might play a role. For the traditional, static $\widetilde{\mathcal{H}}_Q$, it is well-known that 2nd-order perturbation theory yields a correction that shifts the central transition. However, that does not apply here, as the $2\omega_0$ Hamiltonian entails distinct spin operators and components of $\nabla\mathbf{E}$. Nonetheless, a new 2nd-order correction for $\mathcal{H}_{Q2}$ would be of order (ν_{Q2}/ν_0^2), presently about 10^{-5} Hz and negligible compared to the tens-of-Hz broadening we observe.

A fourth notion concerns homogeneity (spatial and temporal) of the $2\omega_0$ $\mathbf{E}$. Sufficient *random* fluctuations of $\mathbf{E}$ or ϕ_E would induce relaxation and line broadening. To explore this possibility, we noted that such effects would appear regardless of *intentional* modulation of ϕ_E, such as a simple case we designed to yield $\overline{\mathcal{H}}_{Q2}^{(0)} = 0$. The conversion $I_{xy}^2 \to I_z^2$ leading to Eq. (2) is valid not only over the full sequence of Fig. 1(a), but also for each triplet of $2\omega_0$ pulses [8]. Thus, inverting ϕ_E on alternate threesomes flips the sign of I_z^2, yielding overall $\overline{\mathcal{H}}_{Q2}^{(0)} = 0$, a phase-modulated control experiment. Fig. 4c demonstrates such refocusing. The usual reference spectrum (no $2\omega_0$ pulses) yielded $\Delta\nu_{ref} = (4.26 \pm 0.08)$ Hz, while the 'Stark-active' result had $\Delta\nu_{Q2} = (17.0 \pm 0.4)$ Hz, similar to the AHT-predicted splitting ($\nu_{Q2} \sim 27$ Hz). In contrast, the phase-modulated control [$\Delta\nu = (4.31 \pm 0.08)$ Hz] was indistinguishable from the reference lineshape, in spite of $2\omega_0$ amplitude (500 V/cm) to match the Stark-active case. Thus, fluctuations faster than $t_{cyc}/4$ do not contribute.

If instead, *drift* in $\mathbf{E}$ or ϕ_E were present, Eq. (2) would predict chirped satellites peaks, but an unchanged central transition. That signature is not apparent in our results. Further, drift was explicitly avoided by using a constant-power format [21] for both $2\omega_0$ and rf magnetic pulses. Finally, spatial variations in $\mathbf{E}$ or ϕ_E would yield satellite broadening, but (as for drift) no effect on the central transition. Here too, inhomogeneity of $\mathbf{E}$ was carefully avoided [17], and its presence would not easily reconcile with our earlier determination of C_{14} by steady state $2\omega_0$ excitation [17,18]. We do note that inhomogeneous $\pi/2$ phase would uniquely impact ϕ_E-coherent POWER experiments, as the $2\omega_0$ phase is defined only relative to that of the magnetic pulses.[1] Nonetheless, we reiterate that such inhomogeneity is not consistent with our observation of broadening that is inclusive of the central transition.

These exclusions leave responsibility for the non-AHT lineshape with higher-order terms [$\overline{\mathcal{H}}_{Q2}^{(n)}$ $(n \geqslant 1)$] in $\mathcal{H}_{Q2,\mathrm{eff}}$. These consist of commutators between 'toggling-frame' forms of I_{xy}^2 (tabulated in Refs. [8,21]). $\overline{\mathcal{H}}_{Q2}^{(1)}$ and other odd-n terms vanish due to symmetry of the design, leaving $\overline{\mathcal{H}}_{Q2}^{(2)}$ as a prime suspect. Cross-term commutators between toggling-frame representations of $\widetilde{\mathcal{H}}'_{Q2}$ and the dipolar Hamiltonian are also of concern, and would represent an interference of the $2\omega_0$ QSE with normal line-narrowing performance. Whatever the origin, unwanted terms might be removed by 2nd-averaging truncation of off-diagonal Hamiltonians. The numerical simulations support that notion, but experiments have

[1] For completeness, imagine $\pi/2$ phase (ϕ_{B1}) that is *in*homogeneous in the lab frame. This would not affect line-narrowing with the bare sequence, as phase of any given $\pi/2$ is defined relative to that of the first pulse. Thus, a local definition of ϕ_{B1} suffices in that case. Now, imagine adding the $2\omega_0$ perturbation with spatially *homogeneous* ϕ_E. Then, in a 'smoothed-frame' of homogeneous ϕ_{B1}, the value of ϕ_E would vary across sample elements, with spins thus experiencing variable $\overline{\mathcal{H}}_{Q2}^{(0)}$ for chirped satellites. Concern over ϕ_{B1} is not general to all POWER experiment types. Rather, it is specific to the $2\omega_0$ case or other synchronizations of resonant, phase-based interactions (including in rf imaging, as per p26 of Ref. [24]).

not as yet succeeded. It may be that 2nd-averaging efficacy is distinct for $\overline{\mathcal{H}}_{Q2}^{(2)}$ vs cross-term contributions, explaining the partial defeat of broadening in numerical simulations and its persistence in experiments. Further study is needed to explore this, including approaches with alternative line-narrowing sequences [21] and/or increased $\pi/2$ amplitudes to approach the infinite-pulse approximation, simplify AHT analysis and make shorter t_{cyc} practical.

In conclusion, we have established phase-coherent QSEs as a new NMR probe of electrostatics. For any spectroscopy, a useful electrostatic probe requires calibrated responses vs both $|\mathbf{E}|$ and its direction. Given such ability, the broad applicability and atomic detail of NMR would provide an ideal approach. Even without phase coherence, rf QSEs are advantageous over static methods due to higher tolerance to $|\mathbf{E}|$ and convenient operation with mostly standard equipment. Furthermore, tensorial definition by prior static or steady state rf methods is laborious and error prone. The POWER method provides ϕ_E as a much more accessible variable than rotation or frequency dependence. Finally, the POWER context promises a degree of linearization in $2\omega_0$ response. Steady state transition probabilities go as $|\widetilde{\mathcal{H}}'_{Q2}|^2$, for Lorentzian response vs $|\mathbf{E}|$ that reduces calibration accuracy compared to linear splitting from static $\mathbf{E}$. POWER NMR can complete the 'secularization' of $2\omega_0$ QSEs by providing a form (I_z^2) with *linear* response to mimic that from the static quadrupolar Stark effect.

Acknowledgments

We thank Prof. Matthias Ernst of the ETH for gamma v4.1.2, Dr. Scott McCallum of RPI for facility support, Dan Weitekamp of Caltech for noting the issue of homogeneity in ϕ_{B1}, and Rensselaer for funding.

References

[1] N. Bloembergen, Linear stark effect in magnetic resonance spectra, Science 133 (1961) 1363–1364.
[2] N. Bloembergen, Electric Shifts in Magnetic Resonance. in: Proc. 11th Colloque Ampere, J. Smidt, (Ed.), North-Holland, Eindhoven, 1962, pp. 39–57.
[3] D. Gill, N. Bloembergen, Linear stark splitting of nuclear spin levels in GaAs, Phys. Rev. 129 (1963) 2398–2402.
[4] E. Brun, R. Hahn, W. Pierce, W.H. Tantilla, Spin transitions induced by external rf electric fields in GaAs, Phys. Rev. Lett. 8 (1962) 365–366.
[5] E. Brun, R.J. Mahler, H. Mahon, W.L. Pierce, Electrically induced nuclear quadrupole spin transitions in a GaAs single crystal, Phys. Rev. 129 (1963) 1965–1970.
[6] J.G. Kempf, D.P. Weitekamp, Method for atomic-layer-resolved measurement of electric polarization fields by nuclear magnetic resonance, J. Vac. Sci. Technol. B 18 (2000) 2255–2262.
[7] J.G. Kempf, M.A. Miller, D.P. Weitekamp, Imaging quantum confinement with optical and POWER (perturbations observed with enhanced resolution) NMR, Proc. Natl. Acad. Sci. USA 105 (2008) 20124–20129.
[8] M.R. Tarasek, J.G. Kempf, A system for NMR stark spectroscopy of quadrupolar, Nucl. J. Phys. Chem. A 114 (2010) 5743–5751.
[9] S.G. Boxer, Stark realities, J. Phys. Chem. B 113 (2009) 2972–2983.
[10] Y. Shen, F. Delaglio, G. Cornilescu, A. Bax, TALOS plus: a hybrid method for predicting protein backbone torsion angles from NMR chemical shifts, J. Biomolec. NMR 44 (2009) 213–223.
[11] I.T. Suydam, C.D. Snow, V.S. Pande, S.G. Boxer, Electric fields at the active site of an enzyme: direct comparison of experiment with theory, Science 313 (2006) 200–204.
[12] R.W. Dixon, N. Bloembergen, Electrically induced perturbations of halogen nuclear quadrupole interactions in polycrystalline compounds. I. Phenomenological theory + experimental results, J. Chem. Phys. 41 (1964) 1720–1738.
[13] R.W. Dixon, N. Bloembergen, Electrically induced perturbations of halogen nuclear quadrupole interactions in polycrystalline compounds 2. Microscopic theory, J. Chem. Phys. 41 (1964) 1739–1747.
[14] M.J. Stephen, The effect of molecular interaction on magnetic shielding constants, Mol. Phys. 1 (1958) 223–232.
[15] A.D. Buckingham, Chemical shifts in the nuclear magnetic resonance spectra of molecules containing polar groups, Can. J. Chem. 38 (1960) 300–307.
[16] K.D. Park, K. Guo, F. Adebodun, M.L. Chiu, S.G. Sligar, E. Oldfield, Distal and proximal ligand interactions in heme proteins – correlations between C–O and Fe–C vibrational frequencies, oxygen-17 and carbon-13 nuclear magnetic resonance chemical shifts, and oxygen-17 nuclear quadrupole coupling constants in $C^{17}O$- and ^{13}CO- labeled species, Biochemistry 30 (1991) 2333–2347.
[17] M.R. Tarasek, J.G. Kempf, RF quadrupolar NMR stark spectroscopy: steady state response and tensorial mapping, J. Phys. Chem. A 114 (2010) 10634–10645.
[18] M.R. Tarasek, J.G. Kempf, Quantitative calibration of radiofrequency NMR stark effects, Rev. Sci. Instrum. 82 (2011) 103904.
[19] H.M. Cho, C.J. Lee, D.N. Shykind, D.P. Weitekamp, Nutation sequences for magnetic resonance imaging in solids, Phys. Rev. Lett. 55 (1985) 1923–1926.
[20] G. Drobny, A. Pines, S. Sinton, D.P. Weitekamp, D. Wemmer, Fourier transform multiple quantum nuclear magnetic resonance, Faraday Symp. Chem. Soc. 13 (1979) 49–55.
[21] M.R. Tarasek, D.J. Goldfarb, J.G. Kempf, Enhancing time-suspension sequences for the measurement of weak perturbations, J. Magn. Reson. 209 (2011) 233–243.
[22] S.A. Smith, T.O. Levante, B.H. Meier, R.R. Ernst, Computer simulations in magnetic resonance. An object-oriented programming approach, J. Magn. Reson. Ser. A 106 (1994) 75–105.
[23] B.J. Soher, K. Young, A. Bernstein, Z. Aygula, A.A. Maudsley, GAVA: spectral simulation for in vivo MRS applications, J. Magn. Reson. 185 (2007) 291–299.
[24] J.A. Marohn, I. Multiple-Pulse Radio-Frequency Gradient Nuclear Magnetic Resonance Imaging of Solids, and II. Optical Nuclear Magnetic Resonance Analysis of Gallium Arsenide Structures, Ph.D. Thesis, Chemistry, Caltech, Pasadena, 1996.